Nuclear Instruments and Methods in Physics Research A 380 (1996) 295–300

NUCLEAR INSTRUMENTS & METHODS IN PHYSICS RESEARCH Section A

ELSEVIER

Mercuric iodide photodetector arrays for gamma-ray imaging

B.E. Patt[a,*], J.S. Iwanczyk[a], Y.J. Wang[a], M.P. Tornai[b], C.S. Levin[b], E.J. Hoffman[b]

[a]*Xsirius, Inc., 1220-A Avenida Acaso, Camarillo, CA 93012, USA*

[b]*Crump Institute of Biological Imaging, UCLA School of Medicine, 10833 Le Conte Ave., Los Angeles, CA 90024, USA*

Abstract

We have developed a novel detector device, namely: a mercuric iodide photodetector array (HgI_2 PDA) to be used with a scintillating crystal for X-ray and gamma-ray imaging. A HgI_2 PDA prototype with 16-pixels has been evaluated with segmented scintillators (CsI(Tl)) coupled to the HgI_2 PDA. Pixel energy resolution of 9.4% FWHM has been obtained at 122 keV for a 4 mm thick scintillator corresponding to 72% stopping at 140 keV, and pixel energy resolution of 11% FWHM has been obtained at 122 keV with the 10 mm thick scintillator.

1. Introduction

Many clinical applications (such as scintigraphy mammography) using conventional nuclear medicine gamma cameras are limited because the conventional gamma camera is limited in performance due to its large size and difficulty in positioning proximally to the organ being diagnosed without the bulk of the body as background. Further limits are in the area of energy resolution and spatial resolution. Energy resolution of about 12% FWHM for the 140 keV photopeak of ^{99m}Tc and spatial resolution of about 4 mm FWHM (intrinsic) is possible for the conventional systems. Moreover, the cost of standard gamma-cameras is high. Small area cameras optimized for particular diagnostic applications can lead to advantages over conventional gamma cameras in terms of both performance and cost.

The current approaches in the development of small cameras for use with low energy X- and gamma-ray emitting radioisotopes such as ^{99m}Tc (140 keV) involve several different technological approaches including new compact position sensitive PMTs (PSPMTs) coupled to scintillator arrays and direct X-ray detectors using room temperature semiconductors such as the high-Z compounds $Cd_{1-x}Zn_xTe$ [1,2] and HgI_2 [3,4].

A new approach which we have investigated is the use of solid state photodetectors coupled with scintillators utilizing a new photodetector array technology, namely: mercuric iodide photodetector arrays (HgI_2 PDA). We have investigated the potential improvements of this technology over the position sensitive PMTs in terms of energy resolution, spatial resolution, and size. Improvement in spatial resolution over existing nuclear medicine gamma cameras results from the better intrinsic detector resolution of the HgI_2 PDA. In addition, the expected improvement in compaction will facilitate closer detector-to-object positioning which can lead to further improvements in the sensitivity and spatial resolution. Improvement in spectral resolution results from the particular parameters of the HgI_2 photodetector such as its very high quantum efficiency and low electronic noise.

Compared with direct X-ray detectors based upon the room temperature high-Z compounds ($Cd_{1-x}Zn_xTe$ and HgI_2), the spectral response of the PDA has advantages in that there is no hole tailing exhibited, and the separation of the photopeak and photofraction are therefore superior. An additional feature is the very weak dependence of spectral characteristics on the thickness of the scintillator. In the case of these direct X-ray detectors, there is a trade off between stopping efficiency (thickness of the device) and spectral quality as the spectral degradation increases rapidly with detector thickness in the 1–4 mm thickness range required at 140 keV. For the PDA/scintillator detector, thick scintillators can be used offering high stopping efficiency without this spectral degradation. The superior energy resolution of this approach, compared with standard gamma-camera technology and other room temperature detectors, can be utilized to enhance image contrast by the rejection of Compton scattered gamma-rays arising from the detector, surrounding collimator and patient scatter environments.

In our current work we have investigated issues to determine the technological requirements necessary for fabricating and assembling the scintillator and photodetector arrays, the optimal choice of components and configuration of the components, techniques for successful integration of the detector components and evaluation of the

*Corresponding author. Tel.: +1 805 484 8300 (ext. 238), fax: +1 805 383 7185, e-mail: 73313.1454@compuserve.com

PII S0168-9002(96)00492-5

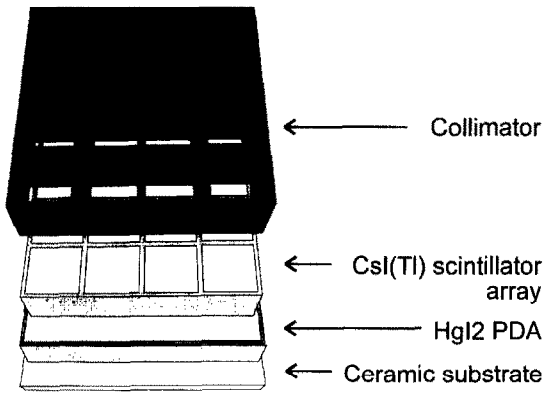

Fig. 1. Schematic diagram of 4-by-4 (16-element) prototypical detector consisting of collimator, scintillator, and HgI_2 photodetector array mounted on ceramic substrate.

performance that can be achieved with prototypical four-by-four (16-pixel) device structures as shown in Fig. 1. This work is intended to allow for development of a scaled-up device with up to 32-by-32 (1024-pixels) elements on a single monocrystalline slice of HgI_2 (>1-in.^{2}) that can be used as the basis for a small imaging device to be used for small field of view imaging or aggregated with more of the submodule devices to form a larger image focal plane.

2. Theory

By using a particular construction the mercuric iodide photodetector technology can circumvent the well known problem associated with trapping of holes in high-Z compound semiconductors. This is because scintillator light photons penetrate only a very shallow region beneath the entrance electrode. When the detector is biased with the entrance electrode negative, only the electrons transit the device and the charge collection (as described by the Hecht relation [5]) becomes essentially single carrier (electron) dominated. This is much closer to the ideal situation as the problems of increased noise due to trapped charge in the direct detectors is due to the significantly lower $\mu\tau$ parameter for holes (ca. 10^{-5} cm^2 V^{-1}) than for electrons (ca. 10^{-3} cm^2 V^{-1}).

The new detector brings together mercuric iodide photodetector and array technologies. Mercuric iodide detectors coupled to CsI(Tl) scintillators have now demonstrated perhaps the best energy resolution at room temperature ever attained by any scintillator/photodetector pair (4.58% FWHM for the 662 keV gammas from ^{137}Cs [6]). In addition, detector designs and fabrication technology have been developed for deposition of segmented electrodes on mercuric iodide, and for optimization of electric fields and minimization of inter-element cross-talk. Smaller active area of the photodetector pixels allows for extremely low electronic noise since the capacitance is very low.

2.1. Energy resolution

The overall spectral linewidth corresponds to broadening of the spectral peaks due to the quadrature sum of factors corresponding to: 1) the electronic noise, which is described below; 2) the intrinsic noise in the scintillator, which is a function of the scintillator material, the photon energy and the geometry of the scintillator, and the surface treatments; 3) the statistical spreading; and 4) the light transfer to the photodetector including the quantum efficiency of the HgI_2 photodetector. The dominant factor varies as a function of energy, with electronic noise dominating at low energies, and intrinsic scintillator noise dominating at high energies. The crossover point at which these contributions are equal has been found empirically to be about 100 keV. Thus for ^{99}Tc Sestamibi studies, lowering of the electronic noise is crucial.

One convenient way to determine the broadening of the photopeak due to electronic noise is to first determine the noise limit for direct X-ray interactions in the HgI_2 detector and then relate this to the photodetector response. The reason for this approach is that the direct response is related to material constants which can easily be measured.

To relate the photoresponse to the direct response, the value of the "direct" noise is scaled by a factor which describes the scaling of the light signal with respect to the direct signal. This factor is inversely proportional to the efficiency for light generation and collection.

The "direct" noise linewidth can be presented as a function of the noise power terms due to the dominant noise sources: series noise, parallel noise, $1/f$ noise and generation recombination noise.

The linewidth (FWHM), ΔE_n, due to the electronic noise (in eV) is [7]

$$\Delta E_n = 2.355\frac{w}{e}\left\{\left[qI'_L + \frac{2kT}{R'_p}\right]\langle N_p^2\rangle + 2kTR'_S C_{in}^2\langle N_s^2\rangle + A_{1/f}\langle N_{1/f}^2\rangle + BC_{in}^2\langle N_{g-r}^2\rangle\right\}^{1/2} \quad (1)$$

where e is the electron charge. Eq. (1) is used with detector leakage current $I_D = 5$ pA, FET gate current $I_g = 0.2$ pA, detector parallel resistance $R_p \sim R_{fb} = 50$ GΩ, where R_{fb} is the preamplifier feedback resistor, FET transconductance $g_m = 5$ mS, FET series noise resistance $R_s = 0.67/g_m$, detector series noise resistance $R_{sd} = 10\Omega$, detector capacitance $C_d \sim 1$ pF, input capacitance (stray

plus FET input capacitance) $C_{in}=3$ pF, and mean energy to create an electron-hole pair $w=4.2$ (HgI_2). A value of ~175 eV FWHM was used for the excess noise due to the FET, feedback resistor, and supporting structures; the generation-recombination noise was ignored, and triangular shaping was assumed.

Because of the low series noise which is a direct consequence of the low detector, input and stray capacitance, and the low parallel noise which results from low detector (and FET) leakage currents, one can achieve a noise limit of ~240 eV FWHM (in "direct" X-ray scale) at a shaping time of ~3 μs at room temperature.

Quantum efficiency of close to 100% has been obtained for HgI_2 photodetectors [8] using various non-metal front contacts such as Hydrogel. However, various concerns about long-term stability and useful temperature range of this material have motivated studies on other contact materials such as ultra-thin metal contacts which are electrically conductive, optically transparent, and non-reactive with HgI_2. Light transmission vs. wavelength and sheet resistance measurements were made for various film thickness. Uniform thin metal films with transmission of about 70% over the range from 450 nm to >1000 nm and with sheet resistance of ~500 Ω/square can be routinely made on HgI_2. These are suitable parameters for the HgI_2 PD.

We have measured ratios in the range of 0.05 for 1 cm thick scintillator coupled to the HgI_2 PD to 0.098 for the 4 mm thick scintillator. Thus the "direct" noise limit of 240 eV implies a "photo" noise level of ~2.5–4.8 keV at room temperature. This corresponds to about 2–4% FWHM contribution to the 140 keV ^{99m}Tc photopeak.

2.2. Spatial resolution

In order to analyze the expected spatial resolution of the PDA it is necessary to include considerations of the collimator and detector specifications and the source-to-collimator geometry. The effects of these parameters on resolution have been well characterized [see for example [9]] for standard nuclear medicine gamma cameras and those principles obtain.

Thus, the system spatial resolution is given as

$$R=\sqrt{R_i^2+R_c^2} \tag{2}$$

where R_i is the intrinsic gamma camera resolution, and the collimator spatial resolution $R_c \approx d(L+z)/L$ with collimator hole diameter d, source to collimator distance z, and hole length L. Considering a source located at a distance of 1 cm from a 2 cm length collimator, spatial resolution of ~3.5 mm is attainable with matched values of 2 mm for the collimator hole diameter and for the intrinsic detector resolution. Spatial resolution under 2 mm is attainable with 1 mm collimator hole diameter and intrinsic detector resolution.

3. Experimental

3.1. Detector fabrication

Although ultimately we plan to investigate the 1 mm collimator hole diameter and intrinsic detector resolution case, the initial work has utilized detectors constructed with 2 mm matched geometry for the definition of the dimensions of the collimator holes, the elements of a segmented scintillator array (with segments optically isolated) such as is available from commercial vendors, and of the electrode patterning of the HgI_2 photodetector array. The spatial resolution in this concept will be identically equal to the geometric spacings of the electrode patterning.

HgI_2 crystals were evaluated and selected. The entrance window was fabricated on prepared crystalline slices by evaporation of an ultra-thin Pd electrode through a physical mask. The requirements for the front contact are optical transparency in the emission band of the scintillator, high electrical conductivity and non-reactive with HgI_2. Pixelation of the front contact is unnecessary as this is accomplished on the back side.

The array has 16-pixels each 2 mm by 2 mm with 0.5 mm gaps between the pixels defined through the geometry of the contact deposition on the back side of the HgI_2 wafer. The thickness of the contact on the back side is not critical. A photograph of the back-side pixelation (seen through the crystal prior to front-side contact deposition) is shown in Fig. 2.

3.2. Scintillator

Segmented scintillators with sixteen CsI(Tl) segments each having 2 mm by 2 mm area with lengths of 4–10 mm CsI(Tl) were procured from Hilger Analytical Ltd. The segments are arranged in a two dimensional 4-by-4 pattern and separated by 0.2 mm septa. The septa are formed by epoxy with TiO_2 doping to enhance reflectivity and to render the septa opaque. The scintillator thicknesses of 4 mm and 10 mm correspond to 72% and >96% stopping (photoelectric) respectively at 140 keV.

3.3. Data acquisition

A test chamber incorporating a platform for the detector followed by sixteen Xsirius designed low-noise charge-sensitive resistor-feedback preamplifiers was used for the measurements. Measurements of individual pixel responses were made sequentially by connecting the sixteen preamplifiers each individually to a Tennelec TC 244 triangu-

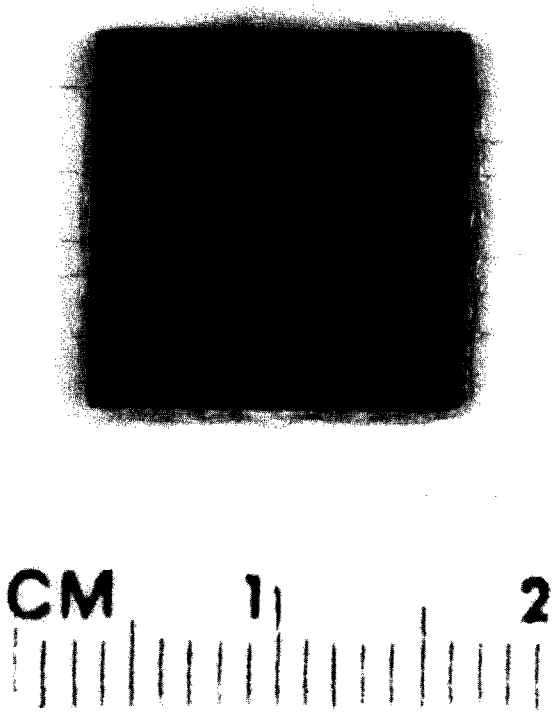

Fig. 2. Photograph of a 4-by-4 prototype HgI_2 PDA during processing showing back-side pixelation (seen through the crystal prior to front-side contact deposition).

lar shaping amplifier. The amplifier output was fed to a standard laboratory Multichannel Analyzer.

4. Results and discussion

4.1. Test chamber noise measurements

The electronic noise inherent in the test chamber was measured by pulser method using the 4-by-4 PDA in the direct X-ray mode and calibrated using the direct ^{55}Fe X-ray response. The average pulser width with full bias on the detector for the 16 channels was about 400 eV FWHM corresponding to about 41 e^- RMS. All components were at room temperature, and the shaping time was 12 μs.

4.2. Evaluation of the pixel spectral response

The response of each of the sixteen individual pixels was measured for ^{241}Am (60 keV photopeak) and ^{57}Co (122 keV) photopeak. In both cases, pixels were irradiated with collimated point sources.

The average energy resolution for ^{241}Am was 13.55% FWHM at 60 keV, and the standard deviation of the resolution values was 0.863% FWHM for the sixteen pixels. A plot of the sixteen pixel spectral response for ^{57}Co is shown in Fig. 3. Shaping time was 12 μs triangular. The average energy resolution was 10.49% FWHM at 122 keV with standard deviation of 0.64% FWHM. Thus we can expect somewhat better than 10% FWHM at 140 keV (energy res. at 140 keV=9.8%= 10.49%×122 keV×sqrt [140 keV/122 keV]/140 keV).

The detailed spectral characteristics of the response for one pixel: *pixel – row 3, column 2* is shown in Fig. 4. The energy resolution of the 122 keV photopeak is 9.4% FWHM. The photofraction measured as the integral counts from 105 keV (14% below photopeak) to 160 keV (30% above photopeak) divided by the integral counts from 20 keV to 160 keV is 80%. The fraction of counts integrated over the region including the Pb K_α, K_β, and Hg and I escape peaks is 12%.

4.3. Resolution vs. shaping time measurements

The ^{57}Co photopeak resolution and electronic noise (pulser method) were measured as a function of shaping time using pixel 3, 2. The minimum electronic noise of about 4.5% FWHM was measured at about 6 μs which agreed with the theoretical prediction. Interestingly, the minimum measured width of the photopeak occurred at the longest shaping time used: 12 μs. Because the electron transit times $T_e = L/(\mu_e E) \sim 0.1$ μs ($L = 1$ mm, $\mu_e = 100$ $cm^2/V\text{-}s$, $E = 20$ kV/cm) are much shorter than the corresponding electron trapping time (10–100 μs), this cannot be accounted for by charge collection in the HgI_2 PDA. Rather, it is likely due to contributions of longer scintillator light production decay components in addition to the published 1100 ns values [10].

5. Imaging

Although the development of a readout system for the PDA/scintillator detector is not yet complete, it was possible to construct images by reading out the individual pixel spectra sequentially and histogramming the integral counts in the photopeak: ~105 keV to ~160 keV for the ^{57}Co source. A lead mask as shown in Fig. 5 (right) was constructed from 2 mm thickness of Pb. Holes of 1 mm diameter were drilled according to the drill pattern shown in the figure.

Aside from the imaging readout system another factor which was not optimal is that only a ^{57}Co point source was available whereas a uniform disk source covering the dimensional area of the detector is required to eliminate angle of incidence effects and produce uniform parallel photon flux. This problem is heightened by the small ratio (0.5) of hole diameter to mask thickness which subtends only a very small solid angle in the source plane.

Nonetheless, a satisfactory first image was obtained

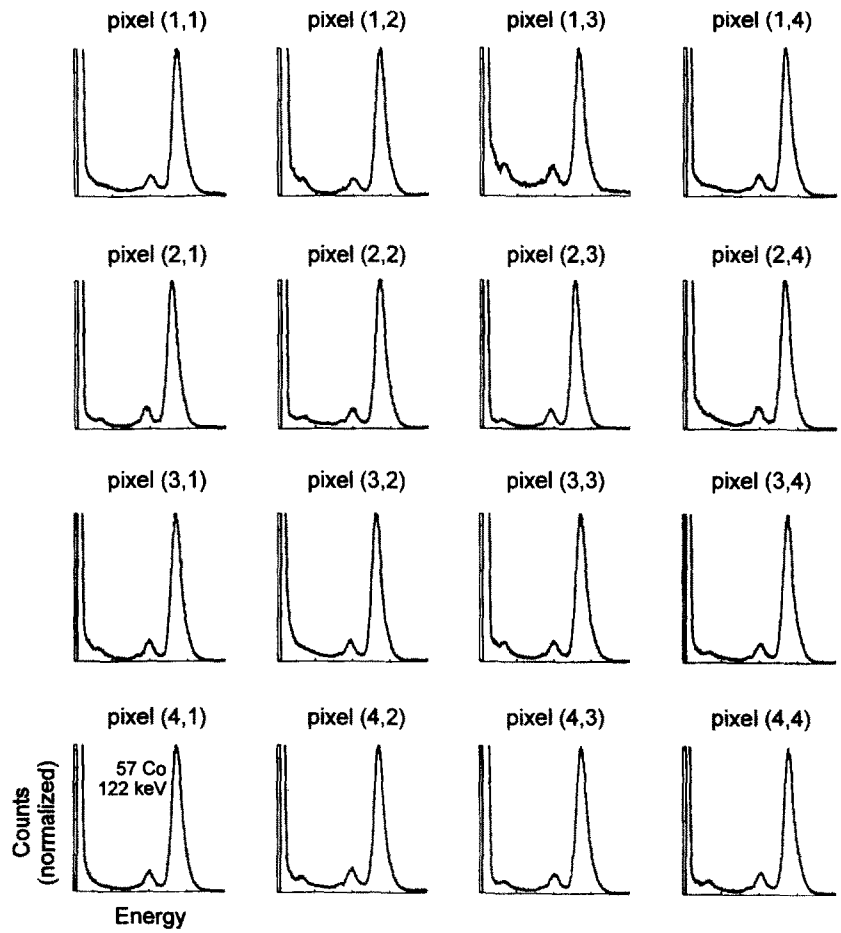

Fig. 3. Gain normalized pixel spectral responses for the ^{57}Co source.

which illustrates the basic functioning of the device for imaging. The pattern of the holes (right) and the corresponding image (left) are shown for a "Xsi" pattern in Fig. 5. The raw image was blurred to remove pixelation effects and contrast was heightened using the transformation $I_o = I_i^X$ where I_o and I_i are the output and input pixel grayscale values respectively, and X is a constant.

6. Conclusions

A mercuric iodide photodetector (PDA) array prototype with 16-pixels each 2 mm by 2 mm with 0.2 mm septa defined through the geometry of the contact deposition on the HgI_2 wafer has been fabricated. The 16-element PDA was evaluated with a segmented scintillator (CsI(Tl)) coupled to the HgI_2 PDA.

Specifications of the device concerning detector performance included sufficient scintillator thickness for at least 1/e photoelectric attenuation in the scintillator, and optimization of the construction of segmented scintillators for maximizing light collection, and spectral match to the photodiode. Theoretical calculations of the expected spectral resolution and spatial resolution were made.

Pixel energy resolution of 9.4% FWHM has been obtained at 122 keV for a 4 mm thick scintillator corresponding to 72% stopping at 140 keV. The measured resolution is consistent with the expected results based upon the theoretical calculations. In addition the first images were obtained with the device. These preliminary results indicate great potential of the proposed approach for imaging X- and gamma rays.

In the future efforts will be aimed at improving further the spectral performance, testing the device with smaller (1 mm by 1 mm) area pixels in order to improve the spatial resolution, and construction of a readout system to simplify image acquisition. Finally, the devices will be examined in terms of their utility towards particular imaging applications in realistic environments.

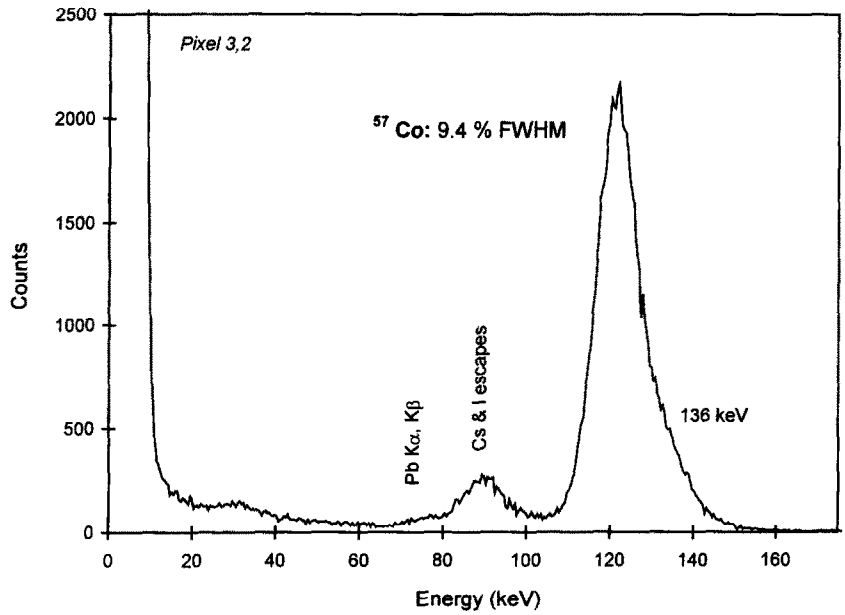

Fig. 4. Spectral detail for representative pixel: row 3; column 2 measured with ^{57}Co source.

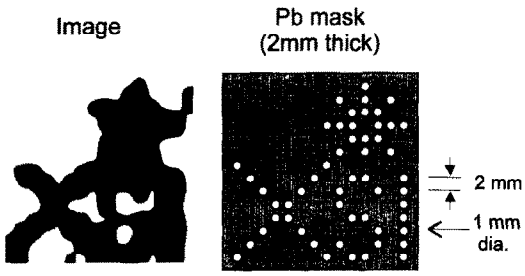

Fig. 5. Pb "phantom" (right) and HgI_2 PDA/CsI(Tl) transmission radiograph acquired using a ^{57}Co source (left).

Acknowledgments

This work was supported by National Institutes of Health, National Cancer Institute Grants # 1 R43 CA68845-01, 2 R44 CA61403-02, and T32-CA09092, and DOE Contract No. DE-FC03-87-ER60615.

The authors wish to thank Mrs. F. Riquelme, Mrs. X. Qin, Mr. J. Menjivar, Mr. G. Maculewicz, Mr. R. Koziol, and Mr. D. Marsh for their assistance with various parts of this work.

References

[1] F.P. Doty, H.B. Barber, F.L. Augustine, J.F. Butler, B.A. Apotovsky, E.T. Young and W. Hamilton, Nucl. Instr. and Meth. A 353 (1994) 356.

[2] J.F. Butler, F.P. Doty, B. Apotovsky and S.J. Friesenhahn, MRS Symp. Proc. vol. 302 (1993) 497.

[3] B.E. Patt, J.S. Iwanczyk, M.P. Tornai, C.S. Levin and E.J. Hoffman, Nucl. Instr. and Meth. A 366 (1995) 173.

[4] B.E. Patt, MRS Symp. Proc. vol. 302 (1993) 43.

[5] J.W. Mayer, in: Semiconductor Detectors, eds. G. Bertolini and A. Coche (North Holland, 1968) chap. 5.

[6] Y.J. Wang, B.E. Patt and J.S. Iwanczyk, IEEE Trans. Nucl. Sci. NS-42(4) (1995) 601.

[7] J.S. Iwanczyk and B.E. Patt, in: Semiconductors for Room Temperature Nuclear Detector Applications, eds. T.E. Schlesinger and R.B. James, Semiconductor and Semimetals Vol. 43 (Academic Press, 1995) pp. 531–560.

[8] J.M. Markakis and A.Y. Cheng, Nucl. Instr. and Meth. A 283 (1989) 236.

[9] R.J. Ott, M.A. Flower, J.W. Babich and P.K. Marsden, in: The Physics of Medical Imaging, ed. S. Webb (Adam Hilger, Bristol, 1988) chap. 6.

[10] Hilger Analytical scintillator catalogues and brochures, 1994–1995.